Second International Symposium on Marine Propulsors
smp'11, Hamburg, Germany, June 2011

Influence of Material and Loading Uncertainties on the Hydroelastic Performance of Advanced Material Propellers

Yin Lu Young[1], Michael R. Motley[1,2]

[1]University of Michigan, Ann Arbor, Michigan, USA
[2]Princeton University, Princeton, New Jersey, USA

ABSTRACT

Composite marine structures are attractive because of their ability to conserve weight, reduce maintenance cost, and improve performance via 3-D passive hydroelastic tailoring of the load-dependent deformations. However, the design of advanced material propellers (AMPs) is non-trivial because of the load-dependent deformation responses that control the propeller performance. The objective of this work is to quantify the influence of material and loading uncertainties on the hydroelastic response and safe operating envelopes of AMPs. A previously validated, 3-D, coupled boundary element method-finite element method (BEM-FEM) is used to analyze the performance of AMPs with consideration for spatially varying flows, unsteady sheet cavitation, material anisotropy, fluid-structure interactions, as well as potential material and stability failures. Results are shown for a pair of carbon-fiber reinforced polymer (CFRP) propellers designed for a twin-shafted naval combatant.

Keywords

Fluid-structure interactions, composite propeller, adaptive structure, reliability, uncertainty

1 INTRODUCTION

Traditionally, marine rotors are constructed from nickel-aluminum-bronze (NAB) or manganese-aluminum-bronze (MAB), materials that provide superior yield strength, corrosion resistance, and affordability. For a designer, the rigidity of a metallic propeller simplifies the design by allowing for separation of the hydrodynamic and structural components. Composite propellers, when compared to their metallic counterparts, can provide weight savings and reduce maintenance cost. In addition, composite propellers can provide improved hydroelastic performance via passive tailoring of the coupled bend-twist deformation responses (Young et al 2006, Young 2008, Liu & Young 2009, Motley et al 2009, Motley & Young 2010a,b,c). Designing an adaptive composite propeller, however, is highly non-trivial because the deformation responses, and hence performance, depend on the total load. For a rigid metallic propeller with diameter, D, the hydrodynamic performance is characterized by the advance coefficient, $J_a=V_a/nD$, which is the *ratio* of the advance velocity, V_a, to the tangential velocity dictated by the rotational frequency, n. For an adaptive propeller, on the other hand, the hydroelastic response depends on the *magnitude* of the advance speed *and* the rotational frequency, and not just on their ratio. Since the deformation changes with loading conditions, which in turn changes the propeller thrust capacity and power demand, as well as cavitation characteristics, it is critical to predict and to optimize the deformation responses over the full range of expected operating conditions.

An additional design consideration for composite materials is their tendency to be more susceptible to material imperfections than metallic alloys due to the complex manufacturing process (Potter 2008). For a composite rotor, random variations due to fiber misalignments, voids, laminate properties, and boundary conditions add another level of uncertainty to the overall propeller response, especially when the performance depends on the deformations, which are governed by the load conditions, material response, and fluid-structure interactions. Hence, the objective of this work is to quantify the influence of material and loading uncertainties on the response, safe operating envelope, and reliability of AMPs.

2 NUMERICAL FORMULATION

A previously developed, fully-coupled, 3-D boundary element method-finite element method (BEM-FEM) is used to analyze the propeller performance. The 3-D

BEM-FEM method is able to consider the effects of nonlinear geometric coupling, fluid-structure interactions (FSI), spatially varying flows, transient fluid sheet cavitation, material anisotropy, as well as potential material and hydroelastic instability failures. The fluid behavior is assumed to be governed by the incompressible Euler equations in a blade-fixed rotating coordinate system. The total velocity is decomposed into an effective inflow velocity that accounts for vortical interactions between the propeller and the inflow, and a perturbation velocity caused by the presence of the propeller that is assumed to be incompressible, inviscid, and irrotational.

The total hydrodynamic pressure and perturbation velocity potential are decomposed into components associated with rigid blade rotation and elastic blade deformation to consider FSI effects. The solid equation of motion is modified to include the spatially and temporally varying added mass and hydrodynamic damping. The commercial FEM solver, ABAQUS/Standard (ABAQUS 2005), is used to solve the modified dynamic equation of motion via user-defined hydroelastic elements and subroutines. Additional details of the formulation, numerical implementation, and validation studies can be found in Young et al (2006), Young (2007), Young and Shen (2007), Young (2008), and Young et al (2008).

3 PROPELLER OPERATIONAL SPACE AND DESIGN

As discussed above, the performance of adaptive propellers depends on the total load and the load-dependent blade deformations, both of which vary with operating conditions. To get an accurate representation of propeller performance over the design life of the structure, the full range of expected operating conditions must be determined based on the vessel resistance and mission profile, as well as anticipated sea conditions. To illustrate the effects of material and loading uncertainties on the hydroelastic performance of AMPs, results are shown in this paper for a pair of CFRP propellers designed for a twin-shafted naval combatant (Motley & Young 2010b,c).

The expected operational space was developed using experimental data for the probabilistic wave height distribution from Ochi (1978) that was converted into a sea state (*SS*) distribution using the Douglas Sea Scale. The probabilistic sea state distribution was coupled with an assumed probability density functions (PDF) of the propeller advance speed, V_a, for different sea states. The resulting joint PDF of the operational space, as shown in Figure 1, is defined as:

$$f_{V_a,SS}(V_a, SS) = f_{V_a}(V_a|SS) f_{SS}(SS) \quad (1)$$

where $f_{Va}(V_a|SS) = P[V_a \in dV_a|SS]$ is the PDF of the advance speed for a given sea state, $f_{SS}(SS) = P[SS \in dSS]$ is the PDF of the sea states, and $f_{Va,SS}(V_a,SS)$ is the resulting joint PDF, shown in Figure 1.

Employing the full-scale vessel resistance, wake fraction, and thrust deduction data for a twin-shafted naval combatant presented in Tsai (1994), combined with an assumed increase in resistance when operating in higher sea states, the probabilistic thrust requirements of the propellers were determined. When coupled with the probabilistic operational space, $f_{Va,SS}(V_a,SS)$, it is possible to derive the expected variation in advance speed and resulting thrust requirements for the AMPs.

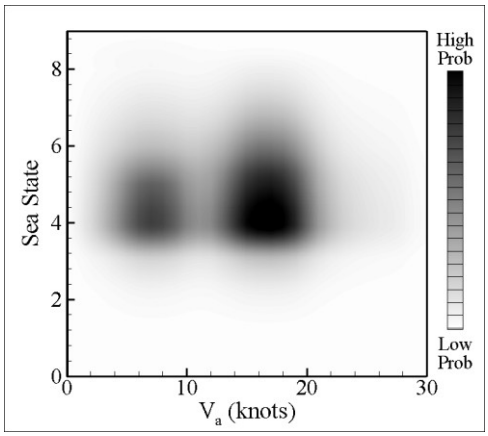

Figure 1: Probabilistic operational space as a function of propeller advance speed and sea state.

The authors have previously designed a pair of AMPs (Motley & Young 2010b,c) for the naval combatant using the assumed probabilistic operational space shown in Figure 1. The geometry and material configuration of the propellers were designed to maximize the lifetime efficiency, defined as the open water efficiency integrated over the entire probabilistic operational space for the vessel. The AMP, shown in Figure 2, was assumed to be made of carbon fiber reinforced polymer (CFRP) with 40% fiber ratio, the material properties of which are given in Table 1. The optimized material stacking sequence for a 10-layer symmetric configuration was found to be $[15^o/30^o/-15^o/0^o/-30^o]_s$.

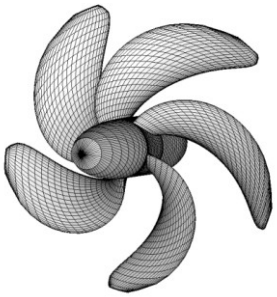

Figure 2: Optimized adaptive propeller geometry.

Table 1: Mean CFRP stiffness and strength parameters

Parameter	Mean	Parameter	Mean
E_1	80.0 GPa	X_T	1950 MPa
E_2	10.0 GPa	X_C	1480 MPa
G_{12}	3.30 GPa	$Y_T = Z_T$	48 MPa
ν_{12}	0.32	$Y_C = Z_C$	200 MPa
ν_{23}	0.32	$S_{XY} = S_{XZ}$	79 MPa
ρ_s	2150 kg/m^3	S_{YZ}	50 MPa

4 WAKE INFLOW ASSUMPTIONS

The authors have previously shown (Young et al 2008, Motley et al 2009, Motley & Young 2010c) that a steady analysis under uniform inflow conditions provides a good approximation of the mean hydroelastic performance of rigid and adaptive propellers under wake inflow conditions, such as the inflow wake shown in Figure 3. To demonstrate, Figures 4-6 compare the mean open water characteristics (thrust coefficient K_T, torque coefficient K_Q, and efficiency η), and variation of the per-blade axial force coefficients and blade tip deformation with blade angle of the optimized adaptive propeller (shown in Figure 2) under uniform (steady) and wake inflow (unsteady) conditions. The results demonstrate that the steady analysis is able to capture the mean response of the propeller behavior under wake flow conditions, and can provide significant computational savings (a few minutes compared to a few hours to reach converged solution for an adaptive propeller). Hence, only steady analysis will be shown herein for the uncertainty analysis.

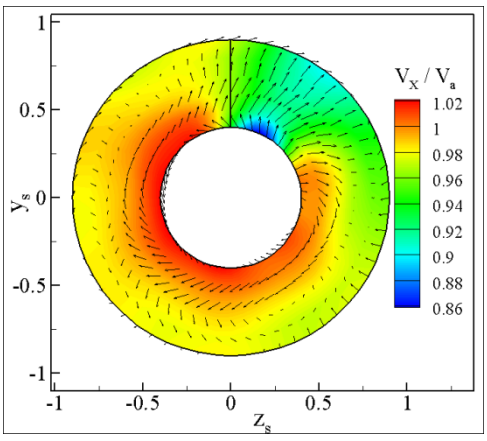

Figure 3: Assumed inflow wake for a dual-shafted combatant craft (Hugel 1992).

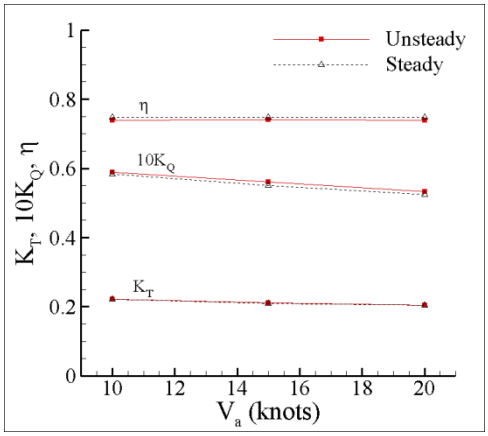

Figure 4: Comparison of mean open water characteristics of the designed propeller under uniform (steady) and wake inflow (unsteady) conditions.

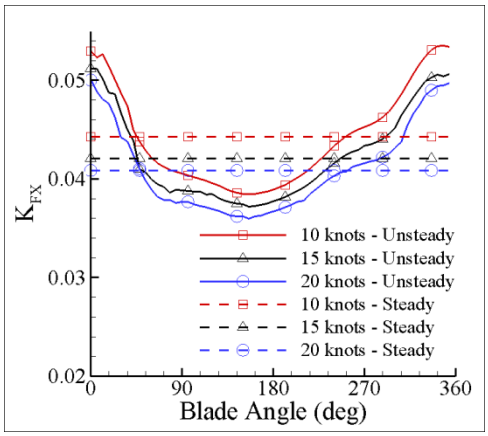

Figure 5: Comparison of the per-blade axial force coefficient based on steady and unsteady analyses.

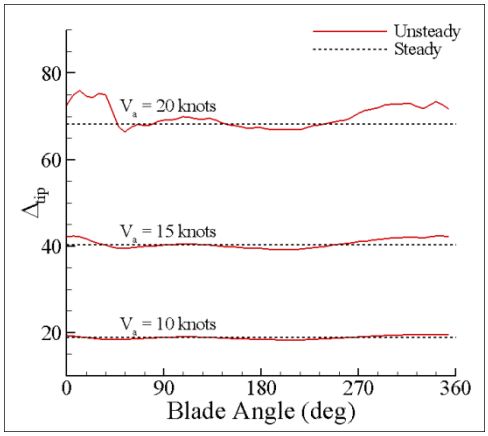

Figure 6: Comparison of propeller tip displacement for steady and unsteady analysis.

5 MODELING MATERIAL VARIABILITY

An AMP blade can consist of tens to hundreds of laminate layers, which is very computationally expensive to analyze if a detailed probabilistic hydroelastic analysis

is needed across the entire operational space. The varying fiber orientations within each laminate layer contribute directly to the overall stiffness distribution and related bend-twist coupling characteristics of the adaptive blades. It has been shown, however, that a multilayer composite laminate can be modeled using an equivalent unidirectional fiber angle, θ_{eq}, which results in approximately the same load-deformation characteristics (Young et al 2008). The 10-layer optimized laminate stacking sequence of $[15^o/30^o/-15^o/0^o/-30^o]_s$ was found to correspond to θ_{eq}=5.0°. Since θ_{eq} is directly a function of both the laminar fiber angle and the corresponding material constituent properties, variability in both laminar fiber angles and material stiffness parameters can be represented through variability in θ_{eq}.

To demonstrate, a Monte Carlo analysis of θ_{eq} was performed by considering random variations in laminate fiber angles and stiffness parameters. Each parameter and fiber angle was given a Gaussian distribution, with coefficients of variation of σ/μ = 0.10 for the stiffness parameters shown in Table 1, and σ/μ = 1° for the laminate fiber angles for each of the ten layers (σ = standard deviation, μ = mean). The resulting probability distribution of θ_{eq}, as shown in Figure 7, has a range of 3.0°-7.0°. It should be noted that in general, a higher θ_{eq} corresponds to a more flexible blade and a lower θ_{eq} corresponds to a stiffer blade in bending along the spanwise direction.

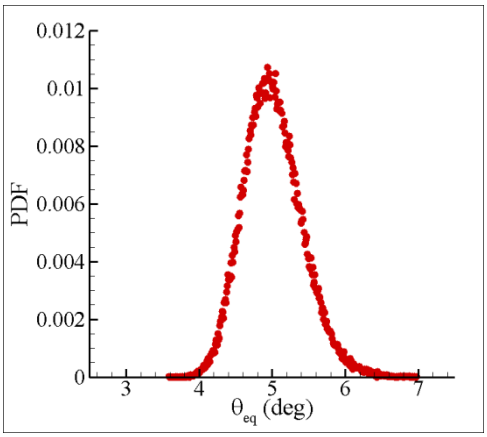

Figure 7: Probability distribution of equivalent unidirectional fiber angles based on Monte Carlo analysis of random variations in material stiffness properties and laminate fiber angles.

Comparisons of the predicted variation of the first three wetted mode shapes and frequencies of the optimized AMP with θ_{eq}=3.0°, 5.0°, and 7.0° are shown in Figure 8. As expected, the fundamental wetted frequency decreased with increasing θ_{eq} due to the increased spanwise bending flexibility.

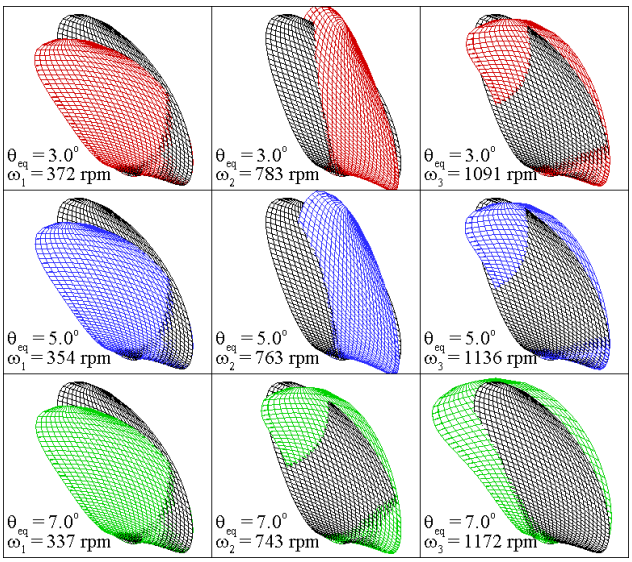

Figure 8: First three wetted mode shapes and corresponding natural frequencies for adaptive propeller blades with θ_{eq} = 3.0°, 5.0°, and 7.0°.

6 STOCHASTIC MATERIAL ANALYSIS

To quantify the effects of material variability on the propeller performance, the 3-D BEM-FEM model was used to compute the load-dependent deformation responses and hydroelastic performance of the AMP blades with θ_{eq}=3.0°, 5.0°, and 7.0°. In doing so, the effects of material uncertainty on the propeller performance across the range of operating conditions can be clearly illustrated. It should be noted that to simplify the analysis, the propeller performance shown herein is based on the operating conditions (i.e., the rotational frequency that delivers the required thrust at the specific advanced speed) for the optimized material configuration of θ_{eq}=5.0°.

6.1 Load-Dependent Deformation Response

Since the performance of an adaptive propeller is dependent on the total load and resulting load-dependent bend-twist deformations, the range of potential blade deformations must be determined. Figures 9 and 10 show the normalized tip deflection, Δ_{tip}/D, and change in tip pitch angle, $\Delta\phi$, respectively, as a function of the advance speed, V_a, corresponding to θ_{eq}=3.0°, 5.0°, and 7.0° for the propeller operating at sea state 2. It should be noted that the trend of the variation of the load-dependent deformation responses are approximately the same for all sea states, and that the deformation increases with increasing sea state due to higher resistance. As expected, the stiffer propeller blade (θ_{eq}=3.0°) provides less deformation, both in bending and twisting, than the optimized material configuration (θ_{eq}=5.0°), and the opposite is true for the more flexible blade (θ_{eq}=7.0°), where both bending and twisting deformations are higher.

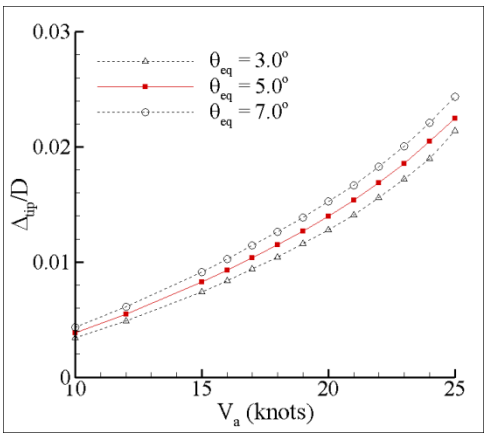

Figure 9: Normalized tip deflection as a function of propeller advance speed at sea state 2 for adaptive propeller blades with θ_{eq} = 3.0°, 5.0°, and 7.0°.

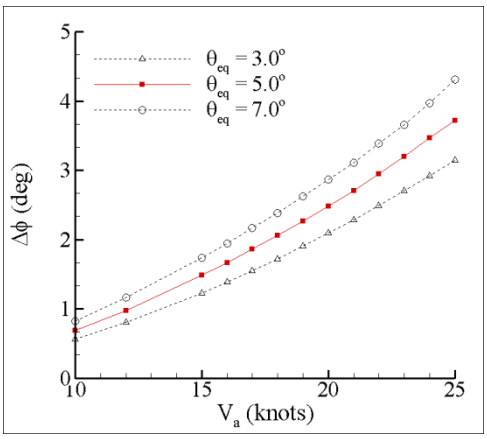

Figure 10: Change in tip pitch angle as a function of propeller advance speed at sea state 2 for adaptive propeller blades with θ_{eq} = 3.0°, 5.0°, and 7.0°.

The variability in load-dependent deformations affects the delivered thrust, T, for a fixed rotational frequency, $n(V_a)$, at a given V_a. Figure 11 shows the variability in T as a function of V_a at sea state 2. As the advance speed increases, the change in delivered thrust increases because the deformation increases with load. Since the blades are designed to depitch, the stiffer blade (θ_{eq}=3.0°) undergoes less deformation, and hence is able to provide more thrust than θ_{eq}=5.0° and 7.0° if $n(V_a)$ is the same for all three material configurations. Since the required thrust as a function of speed and sea state is fixed for a given vessel, the variation in thrust due to material uncertainties will result in inaccurate estimation of the advance speed (as shown in Table 2) unless appropriate changes in the propeller rotational frequency are made to match the required thrust. At low speeds, the difference is negligible; however, the deviation increases with speed, and the difference at the anticipated speed of 25 knots is ±0.35-0.40 knots. To meet the thrust requirement of the vessel, the propeller rotational frequency must be changed from the anticipated values, which will result in changes in efficiency and power requirements, as well as cavitation inception speeds.

Table 2: Variations in propeller advance speed (in knots) due to material uncertainty for adaptive propeller blades with θ_{eq} = 3.0°, 5.0°, and 7.0°.

θ_{eq} = 3.0°	θ_{eq} = 5.0°	θ_{eq} = 7.0°
9.95	10.00	10.06
14.83	15.00	15.12
19.74	20.00	20.27
24.62	25.00	25.34

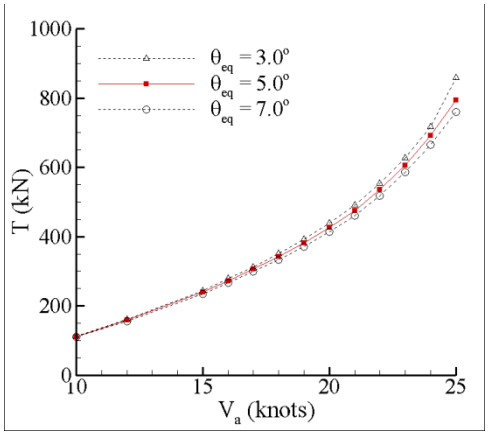

Figure 11: Delivered thrust as a function of propeller advance speed at sea state 2 for adaptive propeller blades with θ_{eq} = 3.0°, 5.0°, and 7.0°.

6.2 Stochastic Reliability Estimates and Safe Operating Envelopes

In addition to changes in the propeller operating conditions in order to match thrust demand of the vessel, variations in material properties and configurations can create uncertainties in safe operating envelopes in terms of cavitation inception and material failure initiation boundaries.

Cavitation inception is very sensitive to changes in effective (deformed) blade pitch angle distribution. In this work, only sheet cavitation is considered, but tip vortex cavitation is expected to be even more sensitive to variations in effective blade pitch angle distributions. The variation in the predicted boundary for the onset of back side fluid sheet cavitation (defined here as when the cavitation volume normalized by R^3 exceeds 1.0e-5, where R is the radius of the propeller) for the designed propeller due to material uncertainty is shown in Figure 12. It is evident that the change in blade stiffness results in a shift in the safe operating envelope for cavitation inception. It should be noted here that the change in tip pitch angle, $\Delta\phi$, is defined as the degree of depitching of the blade, i.e., when $\Delta\phi$ increases, the effective pitch angle ϕ decreases. The more flexible the blade (the

higher the θ_{eq}), the more the blade depitches, and the higher the inception speed for back side sheet cavitation. The resulting shift in the cavitation inception boundary is approximately ±0.5 knots, as shown in Figure 12. By integrating the area of the region to the right of the cavitation boundary under the probabilistic design space, the probability of experiencing cavitation can be determined, and was found to be between 3.0-5.4% depending on the flexibility of the blade, resulting in reliability against cavitation of 94.6-97.0%. It should be noted that the slight nonlinearities in the safe operating envelopes are the result of small fluctuations in the normalized cavitation volume, which is a very small value.

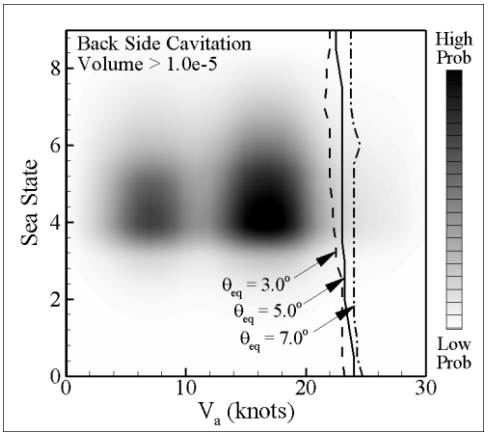

Figure 12: Safe operating boundaries corresponding to the normalized back cavitation volume of 1.0e-5 for adaptive propeller blades with θ_{eq} = 3.0°, 5.0°, and 7.0° within the probabilistic operational space.

In addition to uncertainties in effective material stiffness, another important material uncertainty is the variation in strength, which tends to be greater for composites than metallic alloys. The CFRP blades are made of anisotropic lamina made of fibers and matrix, which have complex failure modes including fiber, matrix, shear, and delamination failure in tension and in compression. The initiation and propagation of the failure mechanisms depend on geometric and material imperfections, manufacturing processes, as well as operating conditions. Further, there are more than 100 models for failure initiation, and each depend on ~5-50 empirically derived constants that may vary with specimen size, construction, and loading conditions. Hence, modeling uncertainties and variability in failure strength parameters are important additional sources of uncertainty that need to be consider when computing the structural reliability.

In general, matrix tensile failure was found to be the dominant failure mode for highly skewed CFRP propeller blades in flexure. Previous work by the authors (Motley & Young 2011) found that the Cuntze failure initiation criteria (Cuntze & Freund 2004) gave the most conservative estimate of matrix tensile failure, and is used for the propeller blades presented herein.

A reliability estimate against matrix tensile failure initiation was calculated by assuming a Gaussian distribution with a coefficient of variation of σ/μ = 0.15 for each of the material strength parameter shown in Table 1, and for each of the three material configurations. A detailed stochastic failure analysis similar to that shown in Motley & Young (2011) was performed for each propeller. A 10,000 simulation Monte Carlo analysis was performed considering random variations in all material strength parameters and estimates of the safe operating envelopes based on probability of failure initiation, P_f, of 0.1% and 1.0% are shown in Figure 13. Blade failure was considered to occur when material failure had initiated in more than 0.05% of the blade. The effects of material strength uncertainties make it more difficult to estimate the total reliability of the blades against material failure within the probabilistic design space. The total probability of failure is determined by finding the probability of failure, $P_f(V_a,SS)$, at each point within the design space and integrating over the entire space. The reliability, R, of the blades can then be defined as:

$$R = 1 - \int_{SS} \int_{V_a} [P_f(V_a, SS) f_{Va,SS}(V_a, SS)] dV_a dSS \qquad (2)$$

It is clear that the change in θ_{eq} has a small effect on the safe operating envelopes. The stiffer blade (θ_{eq}=3.0°) shows a slightly higher susceptibility to failure initiation, which would be expected as higher stiffness results in higher effective pitch angle distributions, which produces higher loads, and hence higher stresses. The resulting reliability against matrix tensile failure initiation is approximately 98.0% (total probability of failure = 2.0-2.1%) for all three material configurations, suggesting uncertainties in material stiffness parameters have a negligible effect on overall system reliability against material failure initiation when compared with uncertainties in material strength parameters.

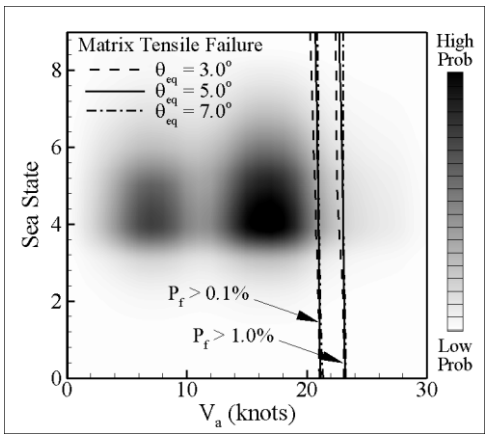

Figure 13: Safe operating boundaries corresponding to probability of matrix tensile failure initiation of 0.1% and 1.0% for adaptive propeller blades with θ_{eq} = 3.0°, 5.0°, and 7.0° within the probabilistic operational space.

It should be noted that the current structural model assumes fixed boundary conditions at the root of the blade, which tends to overestimate the stresses near the blade leading edge and trailing edge at the root due to stress concentrations, as shown in Figure 14 for both the optimized multilayer model and the equivalent unidirectional model. Additionally, because of the use of the effective unidirectional fiber angle, the current material failure initiation limits may be overly conservative; however, detailed studies by the authors have shown the same general trend as discussed herein. A more refined analysis with the appropriate hub attachment details as well as the actual multilayer laminate layup sequence is recommended, but the focus of this paper is to present the methodology and to illustrate the effects of material uncertainty.

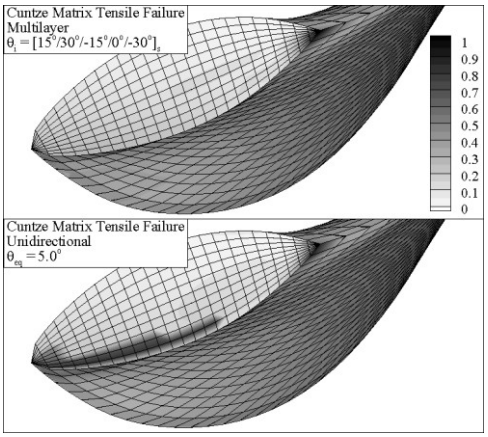

Figure 14: Failure initiation concentrations near the blade leading and trailing edge at the blade root for the multilayer model $\theta_i = [15^o/30^o/-15^o/0^o/-30^o]_s$ and the equivalent unidirectional fiber angle $\theta_{eq} = 5.0^o$.

7 CONCLUSIONS

This paper quantifies the influence of material and loading uncertainties on the hydroelastic response, safe operating envelope, and overall reliability of AMPs. Random variations in laminate fiber angles as well as material stiffness and strength parameters are considered in addition to uncertainties related to material failure initiation models. The effect of material and loading uncertainties on the delivered thrust, advance speed, cavitation inception boundary, and material failure boundary are determined using a previously validated 3-D BEM-FEM model.

The increase in flexibility and dependence on FSI effects makes the design and analysis of adaptive composites highly non-trivial. Additionally, when compared with its rigid metallic counterpart, an adaptive composite propeller is much more susceptible to variability in material configuration, stiffness, and strength parameters, each of which affects the load-dependent FSI response of the propeller blades. The variations in material parameters and material failure initiation models lead to a much wider spread of propeller performance characteristics, operating conditions, and safe operating envelopes for an adaptive propeller compared to a rigid propeller. Hence, it is critical that material and loading uncertainties are considered when designing and analyzing an adaptive composite marine structure whose performance is highly dependent on FSI effects.

ACKNOWLEDGMENTS

The authors are grateful to the Office of Naval Research (ONR) and Dr. Ki-Han Kim (program manager) through grant numbers N00014-09-1-1204 and N00014-10-1-0170 for their financial support.

REFERENCES

ABAQUS (2005), ABAQUS Version 6.5 Documentation. ABAQUS Inc..

Cuntze, R. & Freund, A. (2004). 'The predictive capability of failure mode concept-based strength criteria for multidirectional laminates'. Composite Science and Technology **64**, pp. 344-377.

Hugel, M. (1992). An Evaluation of Propulsors for Several Navy Ships. Master's Thesis, Massachusetts Institute of Technology.

Liu, Z. & Young, Y. L. (2009). 'Utilization of bending-twisting coupling effects for performance enhancement of composite marine propellers'. Journal of Fluids and Structures **25**, pp. 1102-1116.

Motley, M. R., Liu, Z., & Young, Y. L. (2009). 'Utilizing fluid-structure interactions to improve energy efficiency of composite marine propellers in spatially varying wake'. Composite Structures **90**, pp. 304-313.

Motley, M. R. & Young, Y. L. (2010a). 'Reliability-based global design of self-adaptive marine rotors'. Proceedings of ASME 2010 3rd Joint US-European Fluids Engineering Summer Meeting and 8th International Conference on Nanochannels, Microchannels, and Minichannels, Montreal, Canada.

Motley, M. R. & Young, Y. L. (2010b). 'Performance-based design of adaptive composite marine propellers'. Proceedings of the 28th Symposium on Naval Hydrodynamics, Pasadena, California.

Motley, M. R. & Young, Y. L. (2010c). 'Performance-based design and analysis of flexible composite propellers'. Journal of Fluids and Structures, under review.

Motley, M. R. & Young, Y. L. (2011). 'Influence of uncertainties on the response and reliability of self-adaptive composite rotors'. Composite Structures, under review.

Ochi, M. (1978). 'Wave statistics for the design of ships and ocean structures'. Transactions for the Society of Naval Architects and Marine Engineers **86**, pp. 47-76.

Tsai, S., Hopkins, B. & Stenson, R. (1994). 'Comparison of powering performance between DDG-51 and conventional combatant hull forms'. Naval Engineers Journal, September 1994, pp. 88-99.

Potter, K., Khan, B., Wisnom, M., Bell, T. & Stevens, J. (2008). 'Variability, fibre waviness and misalignment in the determination of the properties of composite materials and structures'. Composites Part A **39**, pp. 1343-1354.

Young, Y. L., Michael, T. J., Seaver, M. & Trickey, S. T. (2006). 'Numerical and experimental investigations of composite marine propellers'. Proceedings of the 26th Symposium on Naval Hydrodynamics, Rome, Italy.

Young, Y. L. (2007). 'Time-dependent hydroelastic analysis of cavitating propellers'. Journal of Fluids and Structures **23** pp. 269-295.

Young, Y. L. & Shen, Y. (2007). 'A numerical tool for the design/analysis of dual-cavitating propellers'. Journal of Fluids Engineering **129**, pp. 720-730.

Young, Y. L., Liu, Z. & Motley, M. R. (2008). 'Influence of material anisotropy on the hydroelastic behaviors of composite marine propellers'. Proceedings of the 27th Symposium on Naval Hydrodynamics, Seoul, Korea.

Young, Y. L. (2008). 'Fluid-structure interaction analysis of flexible composite marine propellers'. Journal of Fluids and Structures **24**, pp. 799-818.